Defence Science Journal, Vol. 74, No. 1, January 2024, pp. 22-35, DOI : 10.14429/dsj.74.18460

Experimental and Computing Methods to Determine the External Surface Temperature of the Small Arms Weapon Systems Barrel

M.I. Mărmureanu[#], P. Roșca[#], C. Predoi[#], C.C. Puică[#], A. Malciu[$] and G.F. Noja[#,*]

[#]*Center for Research and Innovation for Armament, Military Equipment and Technologies Research Agency, Bucharest, Romania*

[$]*Doctoral School of Industrial Engineering and Robotics, University Politehnica, Bucharest, Romania*

[*]*E-mail: gnoja@acttm.ro*

ABSTRACT

The need to determine the small arms weapon system barrel temperature under a variety of conditions makes modelling and simulation a good alternative to the expensive real tests. Therefore, in a unique way, this paper includes three alternatives to assess the external surface temperature in order to better understand the balance between the chosen calculation method accuracy and the computed time. For numerical simulations, the initial conditions were established based on STANREC 4367 thermodynamic interior ballistic model. The heat transfer was solved for One-Dimensional and Two-Dimensional model using the finite difference discretisation method, with code written in Matlab. The Three-Dimensional model was resolved by finite element analysis method in Ansys. The simulations results are validated by means of the results obtained in case of two real firing scenarios. During the field testing, a new detection method based on shockwaves microphones was used in order to exactly establish the moment of each shoot and to precisely observe the temperature evolution on barrel surface.

Keywords: Heat; Temperature; Barrel; Matlab; Ansys

NOMENCLATURE

A_w : Chamber wall area plus area of gun tube wall exposed to propellant gases
c_b : Specific heat of the gun barrel material
C_i : Initial mass of igniter
c_p : Specific heat of gas inside the gun barrel
c_T : Total mass of propellant and igniter
E_b : Energy loss due to friction and engraving of rotating band
E_d : Energy loss due to air resistance
E_h : Energy loss due to heat transfer to the chamber and barrel walls
E_p : Energy loss due to propellant gas and unburned propellant motion
E_{pr} : Energy loss due to projectile rotation
E_{pt} : Energy consumed due to projectile translation
E_r : Energy loss due to recoil
F_i : Force per unit mass of igniter
F_p : Force per unit mass of propellant
$GPMG$: General Purpose Machine Gun
h_0 : Free convective heat transfer coefficient for the air inside the gun barrel
h_{int} : Convective heat transfer coefficient inside the gun barrel
Kr : Kurtosis value
L_{sum} : Total work made by gases
M : Mach number
$NRMSE$: Normalised root mean squared error
p_a : Ambient pressure
p_b : Pressure on base of projectile
p_{br} : Resistive pressure of the gun barrel due to friction and engraving
p_g : Pressure of air compressed in front of the projectile
p_m : Space-mean pressure (Noble-Abel Law)
r : Radial coordinate
r_b : Burning law rate (Saint Robert's Law)
R_i : Inner radius of the gun barrel
RMS : Root mean square
S : Surface area of partially burned propellant grain
Sk : Skewness value
S_p : Rojectile cross-section area
t : Time
T_{0_i} : Adiabatic flame temperature of igniter
T_{0_p} : Adiabatic flame temperature of propellant
T_b : Temperature in the gun barrel material
$T_b|_{r=R_i}$: Gun barrel internal wall temperature
T_g : Temperature of propellant gases
$\overline{v}$: Mean cross-sectional flow velocity of gas inside the gun barrel at the fixed axial position
V_c : Volume behind projectile available for propellant gas
V_g : Volume of unburned propellant grain

Received : 23 August 2022, Revised : 02 August 2023
Accepted : 27 September 2023, Online published : 12 January 2024

v_p : Projectile velocity
x : Axial coordinate
x_p : Space travelled by the projectile in gun barrel
Z_p : Relative burnt mass of propellant
γ_a : Ratio of specific heats for air
γ_i : Ratio of specific heats for igniter
γ_p : Ratio of specific heats for propellant
Δr : Radial step (increment)
Δt : Time step (increment)
λ_b : Thermal conductivity of the gun barrel material
λ_N : Nordheim friction factor
$\overline{\rho}$: Mean density of gas inside the gun barrel
ρ_b : Density of the gun barrel material
ω_p : Propellant mass

1. INTRODUCTION

During the firing process, the gun barrel surface temperature increases due to the propellant burning. The magnitude and the three-dimensional distribution of the temperature depends on multiple factors, although the type of ammunition, the rate of fire, the mode of fire and the barrel geometry can be considered major determinants. The flame temperatures and burning characteristics of different ammunition propellant has less influence in case of shooting one bullet. As the number of fired rounds and the firing rate increase, the barrel overheating risk is higher. In such cases, the barrel has a very short time to cool down by natural convection and radiation at its inner and outer surface which leads to heat accumulation, to high and undesirable temperatures. Since the barrel overheating can make the firearm-use dangerous, measurements and analyses have been made over the time to permit the calculation of heat transfer rates and the barrel temperature at any point on it, both in radial and longitudinal position. This data is very important to be known for determining the cook-off temperature, for defining its influence on the barrel strength, for estimating the wear of the bore, for establishing the influence over the firing accuracy or for designing suitable protection elements for handling.

The determination of the barrel temperature can be done both: by theoretical models and by experimental measurement.

Pure theoretical model for a 30 mm caliber gun barrel is identified in[1]. The heat transfer model is formulated and the finite difference method is applied in order to determine the temperature distribution under the single and sequent firing conditions. Also, a one-dimensional analytical model is applied in[2], considering that the heat transfer in the barrel takes place only in radial direction. This solution is compared with others two numerical solving methods, one realized with Matlab software, and other with ANSYS software.

Pure experimental measurement is done on a M16A1 Rifle as part of an improving life program for the barrel. Thirteen thermocouples installed on the top and on the bottom part of the barrel provide information for eight different firing cycles. Round-to-round or burst-to-burst temperature is graphically depicted based on time, in seconds and minutes, which indicates a macro-scale approach[3]. A micro-scale method is done in order to determine the barrel heat transfer of a gun simulator. The instrumentation allows temperature measurements at various location along the interior surface of the 76.5 mm caliber gun barrel, based on a fast-response thin-film resistance thermometer. The data recording at the beginning of each shot is initiated with a photodiode arrangement and the microcomputer samples the signal at a 10 kHz rate. Sensor temperature records at several axial locations are presented till the projectile exit, for 35 millisec., neglecting the barrel heat transfer to the exterior surface of the barrel[4].

Obviously, in both pure cases the absence of experimental measurements or of the theory is felt in the previously references. That is why most of the researches in the ballistic field are based on a mix of theoretical and experimental approach.

The ballistic cycle of the order of milliseconds and the three-dimensional transient phenomenon of the convective heat transfer over seconds, and even minutes in some firing scenarios, make the gun barrel heating a complex process. Therefore, to simplify the computational method and to reduce the computed time, many researchers have developed a one-dimensional method, in cylindrical coordinates, obtaining satisfactory results. Akcay and Yukselen determine the thermodynamic characteristics of the propellant gases and the convective heat transfer coefficient based on the Akcay's internal ballistic code. The predicted temperature of the outer surface is compared with the trial data for a M60 Machine Gun barrel[5]. Ghanem and Abdelsalam came also with a one-dimensional analytical model, completed by tests on a GPMG 7.62X51 mm[6].

For better accuracy, the two-dimensional heat transfer problem from combustion gases to bore surface was studied in[7] using a numerical model to find out the heat flux for GPMG's barrel 7.62×51 mm. A two-dimensional nonlinear thermal conduction model was developed to determine the outside temperature of the barrel for 12,7 mm caliber machine gun[8]. To verify the accuracy of the analytical model, it was performed an experimental test materialised by 120 rounds who was successive fired, with a 3 min. relaxation time for cooling the barrel after firing 60 cartridges. In their paper, Evci and Isik used a three-dimensional unsteady heat transfer computational model in cylindrical coordinates, obtaining results with ANSYS solver[9].

Several common conclusions can be drawn from the analysis of the technical papers presented before. Firstly, the internal ballistic code should be detailed or mentioned as a reference, in order to be completely understood and usable for other researchers. Secondly, the majority of thermal computations is done using an analytical model, or a 1-D, 2-D or 3-D numerical model, with results relating to the maximum values. A third conclusion is that apart from the articles focused only on tests, the others articles briefly present these experimental measurements. More than that, there is no correlation between the moment of the fire and the temperature evolution, the equipment including only a thermal camera or an acquisition system connected to thermocouples.

Therefore, starting from the main purpose of this study, firing scenarios are established in order to determine the exterior surface temperature, both experimentally and theoretically. As part of real test, a new method based on shockwaves is

applied to exactly establish the moment of each shoot. As part of theoretically approach, one objective is to implement the recommendation of STANREC 4367[10] for the thermodynamic interior ballistic model. Another objective is to model and simulate the heat transfer in the small arms weapon systems barrel based on one-dimensional, two-dimensional and three-dimensional heat conduction models.

2. METHODOLOGY

The sub-section "Experiments" describes the instrumentation and the method applied for temperature measurements. The sub-section "Thermodynamic interior ballistic model" reviews the model used to simulate the one-dimensional motion of a projectile inside a gun tube. The third sub-section "Heat transfer simulation" summarises the models and methods for simulating the heat transfer in the small arms weapon systems barrel.

2.1 Experiments

One PA 5.45 mm cal. assault rifle was used for the tests, being installed on a professional weapon test bench (Fig. 1). The instrumentation includes two Optris infrared thermometers, LT CT laser type, with an integrated double laser aiming, installed at a reasonable distance. Together with the mounting bracket that allows the three-dimensional adjustment of the sensor head, a minimum spot as one dot was focused on the barrel surface.

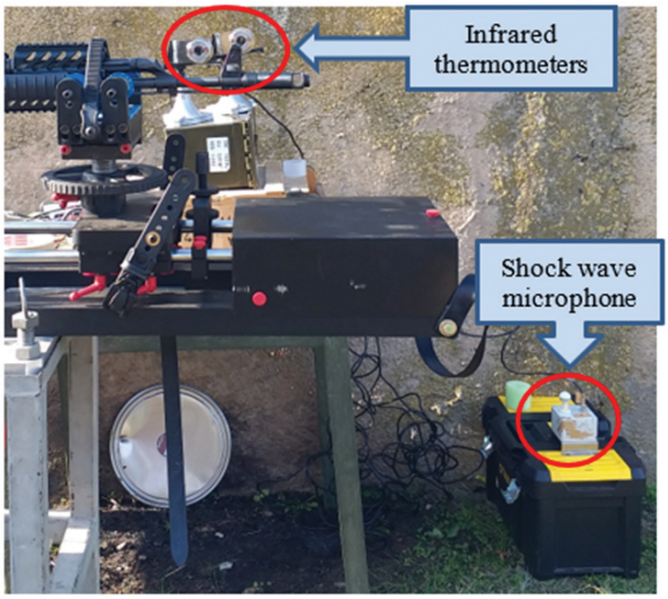

Figure 1. Experimental configuration – the assault rifle, the infrared thermometers and the shock wave microphone.

Figure 2. LT CT laser spots on barrel surface.

In the testing setup two measuring points were considered, the reason for choosing those was generated by the weapon configuration on one hand (exposed part of the barrel) and the position before and behind of the weapon gas port. Clear position of the two port was recorded.

For the two points of interest placed at 57 mm (first point) and 124 mm (sec. point) apart from the weapon muzzle (Fig. 2), the temperature signals are recorded in volts, being scaled to appropriate engineering units – Kelvin degree in this case.

In order to correlate the rise of temperature with the shooting moments, a shock wave microphone was included in the system configuration. The response of the microphone is expressed as a voltage signal, proportional to the shock wave magnitude, with the peak amplitude immediately after the fire pulse.

The BNC jacks allow to connect the signal cables from the infrared thermometers to the input of a NI cDAQ-9171 portable bus-powered USB chassis with the NI 9223 4-Channel, ±10 V, 1 MS/s, 16-Bit, 4-Channel C Series Voltage Input Module. One end of an USB cable is plugged into the NI cDAQ-9171 unit, while the other end is plugged into an available USB port of the processing application host laptop.

The signal cable from the microphone is link to the input of a NI USB-9162 portable bus-powered USB carrier with the NI 9233 4-Channel, ±5 V, 24-Bit IEPE Analog Input Module. One end of an USB cable is plugged into the NI USB-9162 unit, while the other end is plugged into an available USB port of the processing application host laptop.

Since the two NI devices could not be used simultaneous, with the same application and laptop, the configuration presumed usage of two laptops each having connected one NI DAQ board and one trigger connected in parallel to both DAQs in order to simultaneous trigger the recordings. The NI devices configuration and the analogue input data records were made with the help of Analog Input Recorder application from Matlab. A data acquisition frequency of 1.000 Hz was used for the infrared thermometers, while 50.000 Hz was imposed for the microphone, in order to assure proper measurements. Finally, the entire system was prepared for a single shot scenario and a full burst scenario.

2.2 Thermodynamic Interior Ballistic Model

This paper delves into the utilization of the thermodynamic interior ballistic model, wherein global parameters, as defined by the STANREC 4367 lumped-parameters model, are taken into consideration. Notably, this model encompasses the explicit form of the secondary works done by the propellant gases.

The considered model is characterised by a system of non-linear and algebraic equations. These equations serve to replicate the one-dimensional motion of the projectile inside a gun barrel:

2.2.1 Trajectory Equation of the Projectile

$$v_p = \frac{dx_p}{dt} \tag{1}$$

where, v_p is the projectile velocity, x_p is its displacement in gun barrel, t stands for time.

2.2.2 Equation of Motion for a Projectile

$$\frac{dv_p}{dt} = \frac{\left(p_b - p_{br} - p_g\right)}{m_p} S_p \tag{2}$$

where, p_b is the pressure on base of projectile, p_{br} is the resistive pressure of the gun barrel due to friction and engraving, p_g is the pressure of air compressed in front of the projectile and S_p is the projectile cross-section area.

The pressure on the base of the projectile p_b, including the approximate pressure gradient effect is:

$$p_b = \left[p_m + \frac{c_T\left(p_{br} + p_g\right)}{3m_p} \right] \Bigg/ \left(1 + \frac{c_T}{3m_p} \right) \tag{3}$$

where, p_m is the space-mean pressure (Noble-Abel Law) and c_T is the total mass of propellant and igniter.

One strategy used in this model involves adopting a predefined pattern for the resistive pressure $p_{br}(x_p)$. Consequently, until the maximum value is reached the profile used in calculations provides a rapid linear increase, directly followed by a rapid linear decrease to a point which represents that the projectile's engraving into the barrel is completed. After this stage, the system's behaviour is influenced only by the friction between the projectile and the barrel, resulting in a notably slower decrease of the resistive pressure value.

The pressure of air ahead of projectile p_g can be calculated as:

$$p_g = p_a \left\{ 1 + \gamma_a M^2 \left[\frac{1+\gamma_a}{4} + \sqrt{\left(\frac{1+\gamma_a}{4}\right)^2 + \frac{1}{M^2}} \right] \right\} \tag{4}$$

where, p_a is the pressure in the ambient air, γ_a is the ratio of specific heats for air and M stands for Mach number of the projectile with respect to the air.

2.2.3 Propellant Gases Generation Rate Equation

$$\frac{dZ_p}{dt} = \frac{S r_b}{V_g} \tag{5}$$

where, Z_p denotes relative burnt mass of propellant, S is the surface area of partially burned propellant grain, r_b is the burning rate law and V_g is the volume of unburned propellant grain.

2.2.4 Energy Model

$$T_g = \left(\frac{F_p \omega_p Z_p}{\gamma_p - 1} + \frac{F_i C_i}{\gamma_i - 1} - L_{sum} \right) \Bigg/ \left[\frac{F_p \omega_p Z_p}{\left(\gamma_p - 1\right) T_{0_p}} + \frac{F_i C_i}{\left(\gamma_i - 1\right) T_{0_i}} \right] \tag{6}$$

where, T_g is the propellant gases temperature, F_p/F_i is the force per unit mass of propellant/igniter, ω_p is the propellant mass, C_i is the initial mass of igniter, γ_p/γ_i is the ratio of specific heats for propellant/igniter, T_{0_p}/T_{0_i} represents the adiabatic flame temperature of propellant/igniter and L_{sum} represents the total work made by gases.

In the previous section there is loss L_{sum} due to work performed and heat transferred from the system:

$$L_{sum} = E_{pt} + E_{pr} + E_p + E_{br} + E_r + E_d + E_h \tag{7}$$

There are three general classes of loss. The first one is done to the projectile and gun: the energy consumed due to projectile translation E_{pt}, the energy loss due to projectile rotation E_{pr} and the energy loss due to recoil E_r. The second is work lost to the propellants and resistances: the energy loss due to propellant gas and unburned propellant motion E_p, the energy loss due to friction and engraving of rotating band E_{br} and the energy loss due to air resistance E_d. The third is the energy loss due to heat transfer to the chamber and barrel walls E_h.

For the last term of the Eqn. (7), the calculation formula is:

$$E_h = \int_0^t A_w h_{int} \left(T_g - T_b\big|_{r=R_i} \right) dt \tag{8}$$

where, A_w is the chamber wall area plus the area of gun tube wall exposed to propellant gases, h_{int} is the convective heat transfer coefficient inside the gun barrel, r represents the radial coordinate, R_i is the inner radius of the gun barrel (radius of bore) and $T_b\big|_{r=R_i}$ is the gun barrel internal wall temperature.

According to STANREC 4367 provisions, an approximation for the convective heat transfer coefficient inside the gun barrel is

$$h_{int} = \lambda_N \bar{\rho} c_p \bar{v} + h_0 \tag{9}$$

where, $\bar{v}$ represents the mean cross-sectional flow velocity of gas inside the gun barrel at the fixed axial position, $\bar{\rho}$ denotes the mean density of gas inside the gun barrel, c_p represents the specific heat of gas inside the gun barrel and h_0 is the free convective heat transfer coefficient for the air inside the gun barrel (here maintained constant at 11.35 W/m^2·K). The Nordheim friction factor, λ_N, is a dimensionless constant which is approximated by:

$$\lambda_N = \left[13.2 + 4\log\left(200 R_i\right) \right]^{-2} \tag{10}$$

2.2.5 Equation of State

$$p_m = \frac{T_g}{V_c} \left(\frac{F_p \omega_p Z_p}{T_{0_p}} + \frac{F_i C_i}{T_{0_i}} \right) \tag{11}$$

where V_c is the volume behind projectile available for propellant gas.

The Eqn. of state utilises the Noble-Abel Law to compute the space-mean chamber pressure of the ballistic system.

To account for the temperature distribution along the inner wall of the barrel, the heat Eqn. in cylindrical coordinates were alternatively solved using numerical methods, starting with the initial condition value $T_b\big|_{r=R_i}$ known from the interior ballistic model results:

- One-Dimensional Heat Conduction Eqn.

$$\frac{\partial T_b(r,t)}{\partial t} = \frac{\lambda_b}{c_b \rho_b} \left[\frac{\partial^2 T_b(r,t)}{\partial r^2} + \frac{1}{r} \frac{\partial T_b(r,t)}{\partial r} \right] \tag{12}$$

where, T_b is the temperature in the gun barrel material, λ_b represents the gun barrel material thermal conductivity, c_b is the gun barrel material specific heat and ρ_b represents the gun barrel material density.

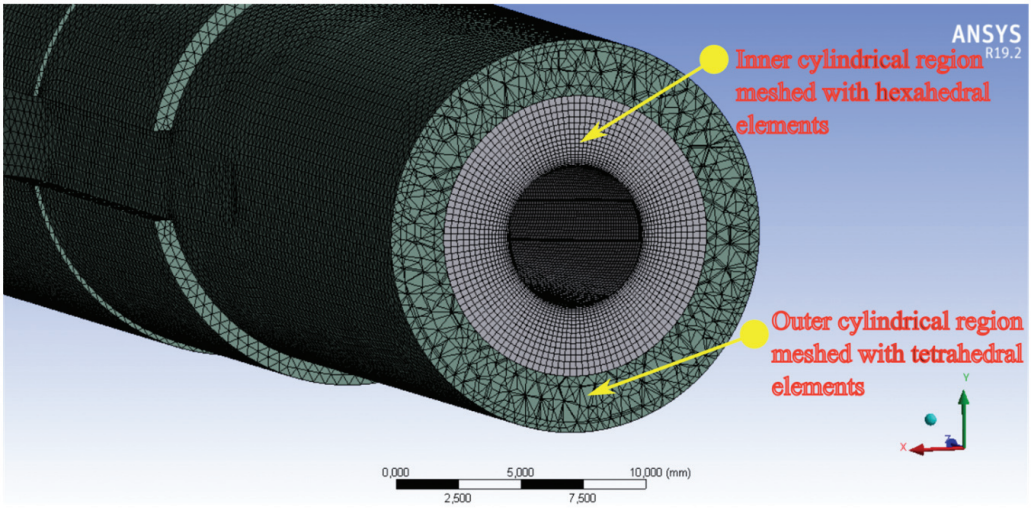

Figure 3. The discretisation of the two regions of the gun barrel.

Table 1. Thermophysical properties for the steel barrel[13]

Temperature [K]	Thermal conductivity$^{W/m\cdot K}$	Specific heat$^{J/kg\cdot K}$	Density [kg/m^3]
293	33.8	480.3	7801
573	32.0	538.2	7801
873	31.0	595.1	7801
1173	30.5	634.2	7801

- Two-Dimensional Heat Conduction Eqn.

$$\frac{\partial T_b(x,r,t)}{\partial t} = \frac{\lambda_b}{c_b\rho_b}\left[\frac{\partial^2 T_b(x,r,t)}{\partial r^2}+\frac{1}{r}\frac{\partial T_b(x,r,t)}{\partial r}+\frac{\partial^2 T_b(x,r,t)}{\partial x^2}\right] \quad (13)$$

where x is the axial coordinate.

In the process of modelling the phenomenon, the assumption was made that the gun barrel wall material is uniform, and there is no presence of protective coatings like galvanic chrome or a nitrated casing on the inner surface of the gun barrel.

The flowing of propellant gas in gun barrel belongs to forced convection, which neglects the radiation heat transfer as the gun barrel belongs to closure space in the period of interior ballistic. Subsequent, it is considered that the gun barrel will exhaust all the propellant gas and filled with air of ambient temperature after the end of the interior ballistic period.

2.3 Heat Transfer Simulation

2.3.1 One-Dimensional and Two-Dimensional Models

The mathematical models with one-dimensional and two-dimensional heat conduction for gun barrel were used. In both cases, the finite difference equations governing the internal nodes were derived by applying the FTCS (Forward Time Central Space) scheme. Additionally, considering convective boundary conditions, finite difference schemes for both internal and external nodes were developed using the energy balance method. A following division for gun barrel was assumed: into 60 sections along the radius and into 503 sections along the axis (barrel length) x. For this, the temperature distribution of the gun barrel was calculated numerically by Matlab programming based on the numerical results of the interior ballistics with lumped-parameters model.

The time and radial steps are conveniently chosen so that:

$$\Delta t \le \frac{c_b\rho_b}{2\lambda_b}(\Delta r)^2 \quad (14)$$

For one-dimensional heat conduction Eqn. and

$$\Delta t \le \frac{c_b\rho_b}{4\lambda_b}(\Delta r)^2 \quad (15)$$

For two-dimensional heat conduction Eqn.

2.3.2 Three-Dimensional Model

In order to observe the temperature distribution through the gun barrel in a three-dimensional model, a Transient Thermal Analysis module was set up in ANSYS workbench. Hence, a 3-D model of the gun barrel was built using SolidWorks, that was firstly imported in ICEM CFD for discretisation. The barrel was divided in two cylindrical regions: the inner one having a thickness of 2,66 mm for both Point 1 and Point 2 sections; the outer region has had 1,61 mm thickness in the Point 1 section and 2,34 mm in the Point 2 section. These two regions were created because, according to[11], the region where the heat flux vector is expected to rapidly change its value should be discretised with a finer mesh. Also, according to[12], the hexahedral elements were applied for the inner region in order to obtain more accurate results. In the outer cylindrical region, the heat flux vector has smaller values than those from

the vicinity of the barrel inner surface, allowing a coarser tetrahedral element mesh type in order to reduce the time computation costs. Finally, it results a mesh with 4.752.795 elements and 3.243.309 nodes (Fig. 3).

The discretised 3-D model was after imported in a Transient Thermal module, the next steps being necessary in order to solve the problem:

- The ambient air temperature is defined as in reality.
- The gun barrel material is stated: steel, defined by the thermophysical properties as shown in Table 1.
- The barrel is divided in 11 target regions (Fig. 4) in order to apply the thermal loadings according to the interior ballistic phenomenon.
- A heat flux loading is applied on the barrel inner surface by defining 11 Heat Flux components (Fig. 4) according to the values obtained for the burned gas heat flux from the thermodynamic interior ballistic model (Table 2).
- The heat flux time evolution for one round burst can be observed in the graphs shown in Fig. 5 and Fig. 6.
- A permanent convection component is also defined on the whole barrel outer surface, in order to simulate the heat convective transfer between the barrel and air for the total time of burst; the convective heat transfer coefficient has been settled by using the temperature dependent tabular data provided by ANSYS Workbench library for Stagnant Air – Horizontal cylinder, as it is described in the Table 3.
- Considering the objectives of this work, only the heat transfer problem was followed to be solved; for that reason, the thermal stress computation option, provided by ANSYS in the Transient Thermal module, was disabled.

3. RESULTS

3.1 Experimental Results

Measurements include the single shot scenario and the full burst scenario at a 280.15 K ambient temperature. The variation of the temperature at the two measurement points along the barrel is graphically presented in Fig. 7 for burst controlled firing. The shooting generated signal was recorded in volts and plotted as vertical lines.

The initial barrel temperature was different at the two points of interest since previously shootings have been done in order to verify if setup of thermal sensors is correct. An increase of 2 K average value is observed at every shoot fired. Interesting to notice is the immediately de grease of barrel temperature of about 0.3 K after each fire.

For the full burst scenario, test data were captured for 30 rounds burst. A medium value of 709 rounds per minute was obtained after data processing. Figure 8 plots the temperature and the successive firings against the time.

The full burst scenario was performed after some single shot scenarios, the weapon not being allowed to fully cooled down to the same initial temperature as the single shot one. During the 30 rounds full burst, 53 K increase is determined for the closest point to the weapon muzzle and 49 K increase for the second point. The magnitude rapport is changed after a second from the last shoot when the temperature increase is stopped, due to thermal inertia of the barrel material. Finally, a 63 K, respectively 79 K increase of temperature is obtained for the barrel exterior surface in the two measured points. The immediately degrease of barrel temperature is also observed at the beginning of the shooting. Apart from this initially decrease, a linear increase of temperature is observed with a 24 K/s gradient.

One possible explanation for initial temperature drop could be the fact that the gun fired from a gun rest that is moving back and forward due to recoil forces, this contributing furthermore to barrel cooling. Another element is that, on initial firing, due to metal thermal inertia, the heat generated by the firing phenomenon need some time to get from inside to outside of the barrel. The same phenomenon was observed when inspecting another gun barrel temperature during controlled burst shots using a MWIR thermal camera as can be seen in Fig. 9, and completely without any relation between experiments.

Similar drops were revealed in[4], in the late of 80 thies, with the explanation that the deviation from zero in the first milliseconds of each trace is within the experimental uncertainty of the sensor. The explanation given in[4] could not be taken as plausible since the same phenomenon was observed 40 years later using more advanced sensors and recording systems. Obviously, further experimental shootings should be conducted in order to validate or invalidate the previously mentioned suppositions and also more investigation to be done in order to determine the exact cause of this observed temperature drop.

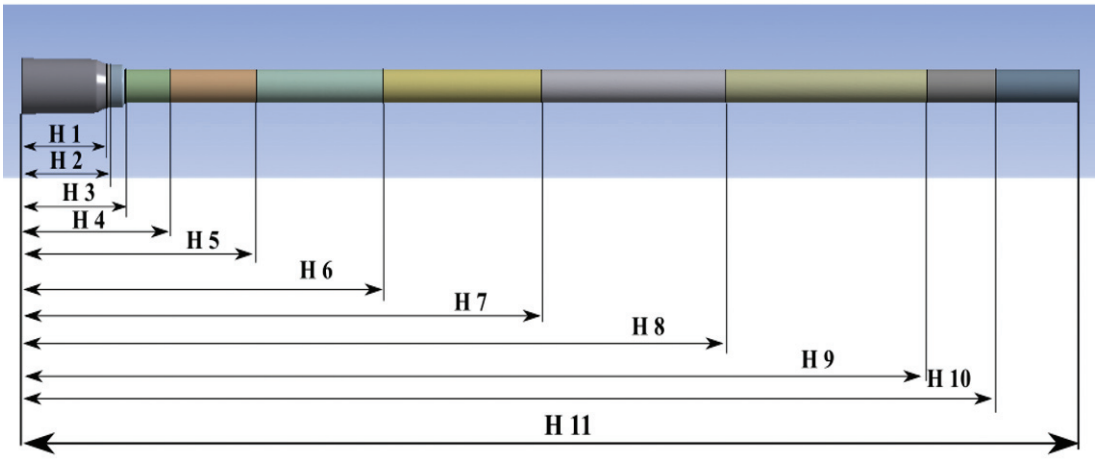

Figure 4. The target regions selected for the heat flux components application.

Table 2. Thermodynamic interior ballistic model results for the burned gas heat flux

Period	Time^{s}	Heat flux$^{W/m2}$	Bullet position in the barrel^{mm}	Region
	0	40665,33265	0	**H 1**
	0,0001	2531647,761	0,279334	**H 2**
	0,0002	35924068,06	1,711392	**H 3**
	0,0003	310837949,6	7,723043	**H 4**
	0,0004	868583231,5	25,10795	**H 5**
When the bullet travels through the barrel	0,0005	833102644,7	58,86927	**H 6**
	0,0006	542561586	108,264	**H 7**
	0,0007	377550923	170,2074	**H 8**
	0,0008	220240653,4	241,9305	**H 9**
	0,0009	127921136	320,5518	**H 10**
	0,000975	96965145,26	381,38	**H 11**
	0,000975	96965145,26	381,38	**H 11**
	0,00148	54060770,57	381,38	**H 11**
	0,00198	19245361,1	381,38	**H 11**
	0,00248	5974072,051	381,38	**H 11**
	0,00298	1642551,74	381,38	**H 11**
	0,00348	393708,499	381,38	**H 11**
	0,00398	74425,5398	381,38	**H 11**
	0,00448	5355,376874	381,38	**H 11**
After the bullet exits the muzzle	0,00498	-4639,473257	381,38	**H 11**
	0,00548	-3629,559152	381,38	**H 11**
	0,00598	-1878,678667	381,38	**H 11**
	0,006185	-1373,007365	381,38	**H 11**
	0,00669	-1733,5573	381,38	**H 11**
	0,00719	-2053,954024	381,38	**H 11**
	0,00769	-2340,60444	381,38	**H 11**
	0,00774	-2366,120319	381,38	**H 11**
	0,08463	-563,536149	381,38	**H 11**

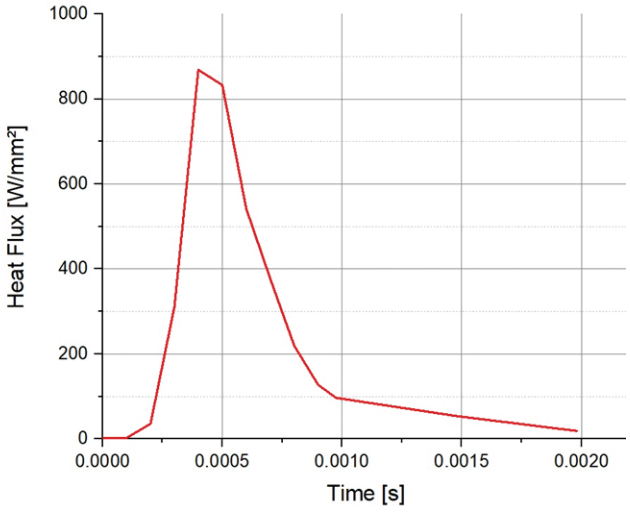

Figure 5. Heat flux vs time, for the period while bullet travels through the PA's barrel at 280.15 K ambient temperature.

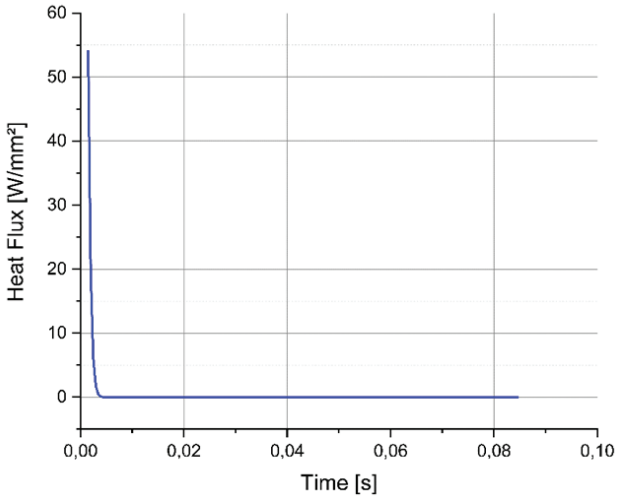

Figure 6. Heat flux vs time, for the period after the bullet exits from the PA's muzzle at 280.15 K ambient temperature until the next bullet is initiated .

Table 3. Tabular data for temperature dependent convection coefficient

Temperature^{K}	Convection coefficient$^{W/mm2\cdot K}$
274,15	1,24e-006
283,15	2,67e-006
373,15	5,76e-006
473,15	7,25e-006
573,15	8,3e-006
773,15	9,84e-006
973,15	1,101e-005
1273,2	1,24e-005

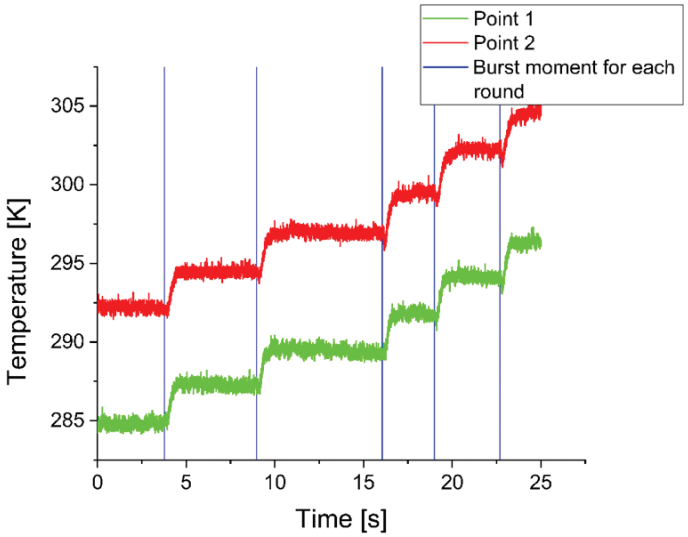

Figure 7. Temperature increase for single shot scenario.

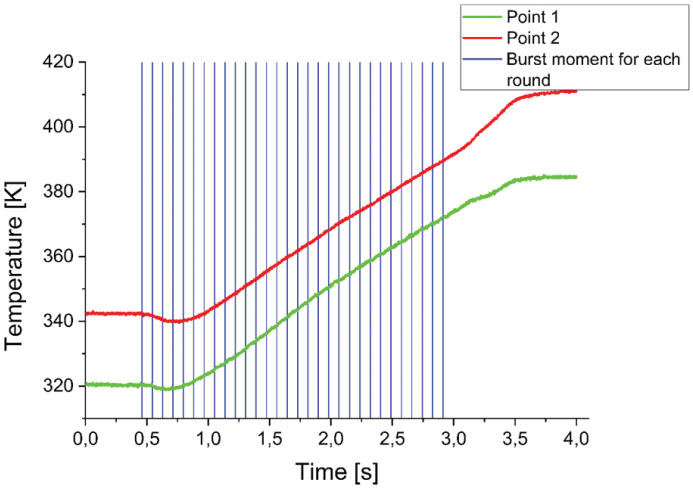

Figure 8. Temperature increase for 30 round burst scenario.

3.1.1 One-Dimensional Model Results

3.1.1.1 Single Shot Scenario

In this case, the results of the 1-D model simulation regarding the temperature variation by time, saved on the two temperature probes, denoting Point 1 and Point 2 from the experiments, can be observed on the graphs presented in Fig. 10. The simulation was performed on a 4 cores Intel-Core i7 CPU computer, 8 GB RAM, and the convergence time was approximately 7 min.

3.1.1.2 Full Burst Scenario

In this situation, the results of the 1-D model simulation regarding the temperature variation by time, saved on the two temperature probes, denoting Point 1 and Point 2 from the experiments, can be observed on the graphs presented in Fig. 11. The convergence time was approximately 1 min.

3.1.2 Two-Dimensional Model Results

3.1.2.1 Single Shot Scenario

For this scenario, the results of the 2-D model simulation regarding the temperature variation by time, saved on the two temperature probes, denoting Point 1 and Point 2 from the experiments, can be observed on the graphs presented in Fig. 12. The convergence time was approximately 1.5 hrs.

3.1.2.2 Full Burst Scenario

As it was done for the single shot scenario, the results of the 2-D model simulation regarding the temperature variation by time, saved on the two temperature probes, denoting Point 1 and Point 2 from the experiments, can be observed on the graphs presented in Fig. 13. The convergence time was approximately 17 mins.

3.1.3 Three-Dimensional Model Results

As it was upper presented, the scope of Transient Thermal Analysis was to model the heat transfer in a gun barrel in a three-dimensional approach. Hence, the two firing scenarios, described in the experiments section, were used for the finite element model set up.

First of all, the two points indicated on the test gun and used for temperature infrared measuring have been simulated by inserting a temperature probe for each other, at the same distances from the muzzle as it was settled in the experiment (Fig. 14).

3.1.3.1 Single Shot Scenario

For the 5 rounds shot in single shot regime, the next supplementary data and steps were defined before the simulation execution:

- The ambient air temperature was set to 280.15 K, considering the weather conditions recorded at test range location;
- The initial temperature of the gun barrel steel has been set at a constant value of 280.15 K along barrel length;
- As it can be seen in Fig. 15, the next steps were also needed to be done:
  - Taking into consideration that the initial temperature at the two points was different at the moment of firing in the experimental tests, a Transient Thermal module was set with the heat flux values presented in Table 2 and distributed accordingly to the 11 regions described above, in order to simulate several successive rounds burst;
  - After the burst simulation setup, a Convection component, applied on all surfaces of the barrel,

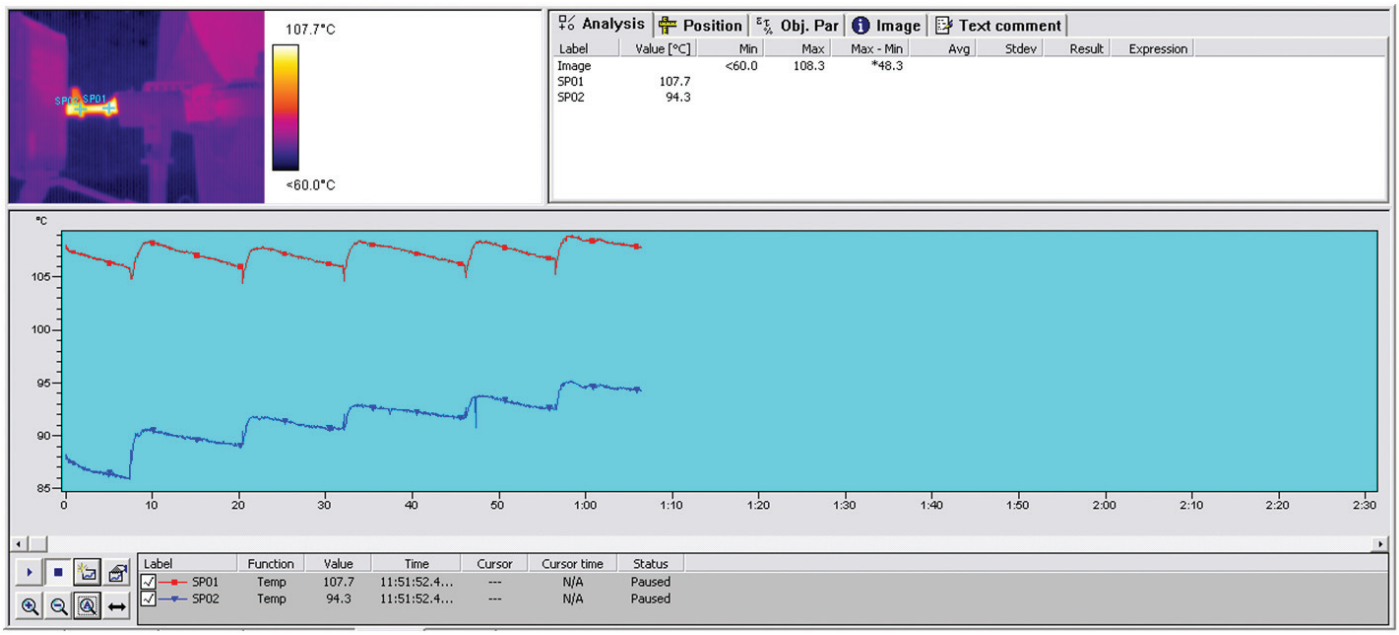

Figure 9. Gun barrel temperature measurement using a MWIR thermal camera.

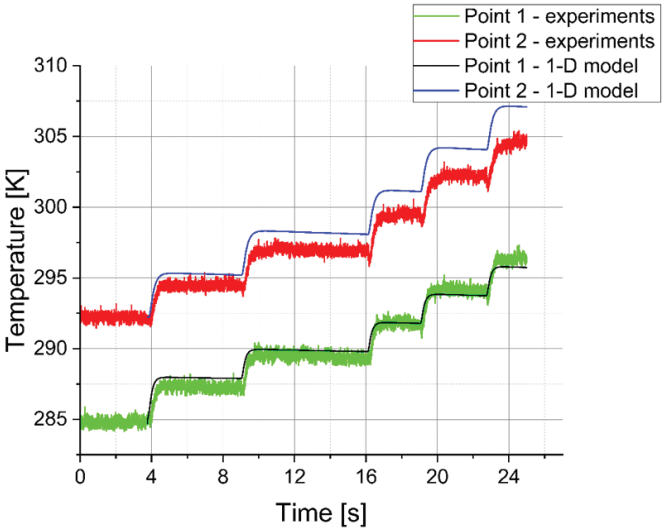

Figure 10. 1-D model simulation temperature, single shot scenario.

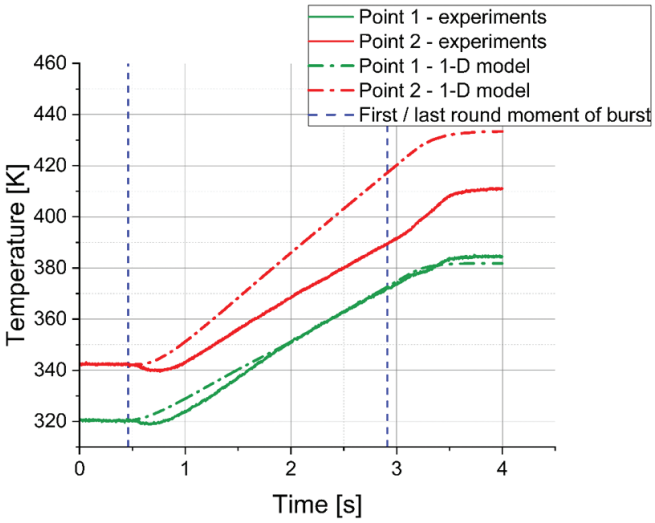

Figure 11. 1-D model simulation temperature, full burst scenario.

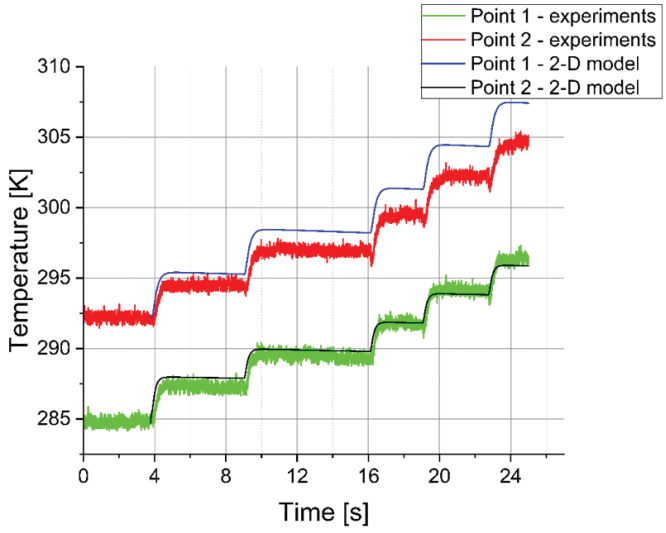

Figure 12. 2-D model simulation temperature, single shot scenario.

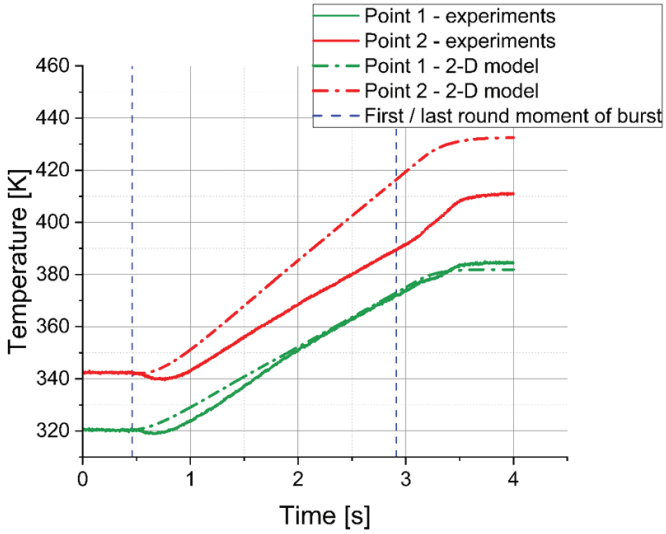

Figure 13. 2-D model simulation temperature, full burst scenario.

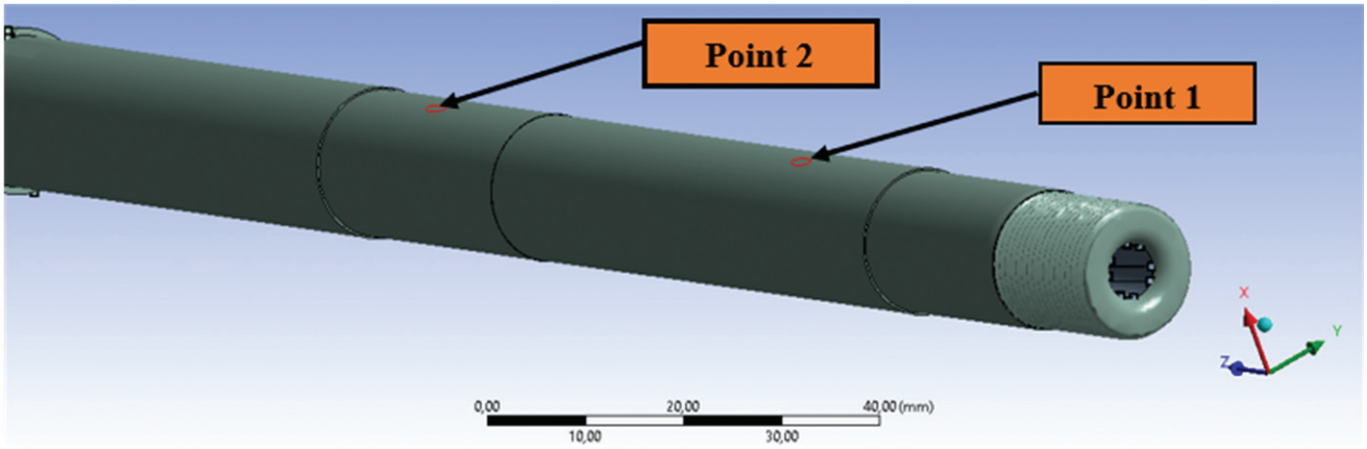

Figure 14. The positioning of the temperature probe.

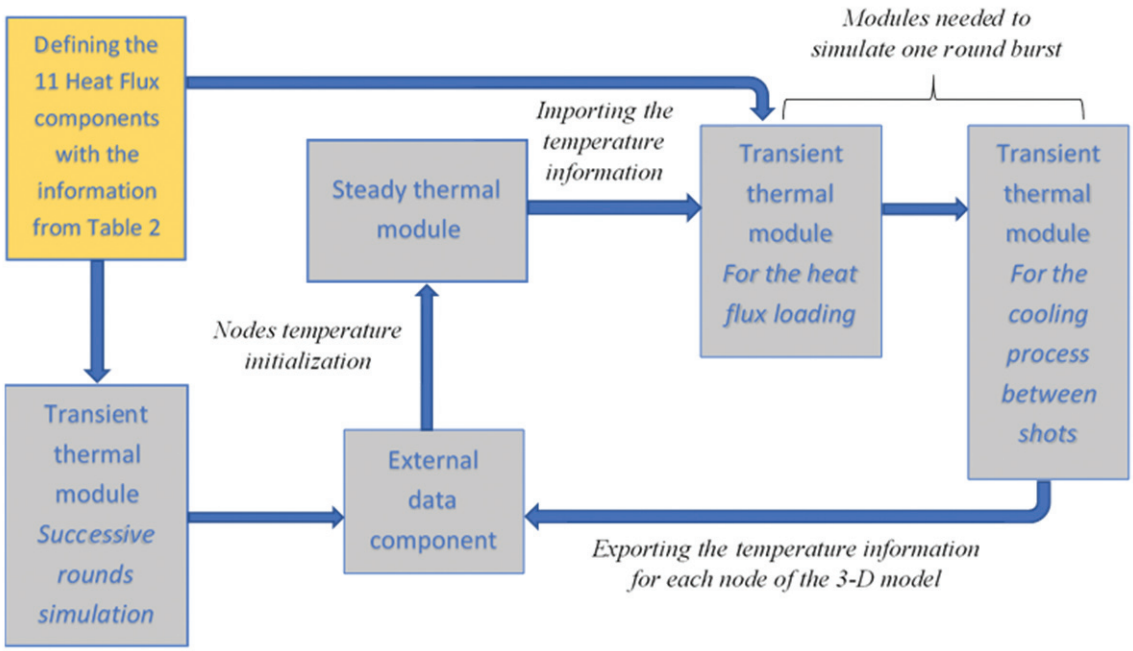

Figure 15. The 3-D simulation process.

was also defined by selecting the Stagnant Air – Horizontal Cylinder option, being executed until the difference of approximately 7.4 K was reached;

- After that, the temperature information for each node were exported to an external data component to define a Steady Thermal module that was only used to initialize the temperature of the whole 3-D model of the barrel from Transient Thermal module;
- Next, the Transient Thermal module was defined with the 11 *Heat flux* components and a Convection one by introducing the values from Table 2 and 3; beside that, in order to simulate the cooling process between rounds, another Transient Thermal module was set with a Convection component, defined as it is previously said in the methodology section, being scheduled to run after the first one; once the setup of the modules was done, the simulation of a single shot was executed.
- The cooling module was set by applying Convection component on the inner and the outer surfaces of the barrel; the convective heat transfer coefficient was defined with the data contained in Table 3;
- After each simulation of cooling process, the nodes temperature information obtained from previously point was again exported in the External Data component that was used for the reinitialization of the 3-D model nodes temperature distribution for the next round burst simulation;
- The work described at previously steps and explained in Fig. 15 was repeated for each single shot simulation, the duration between two successive rounds being the only parameter that was modified having the values noticed in the experimental results.

In this case, the results of the 3-D model simulation regarding the temperature variation by time, saved on the two temperature probes, denoting Point 1 and Point 2 from the experiments, can be observed on the graphs presented in

Fig. 16. The simulation was performed on a 32 cores CPU plus 1 core Nvidia GPU server with 256 GB RAM and convergence time was approximately 50 hrs.

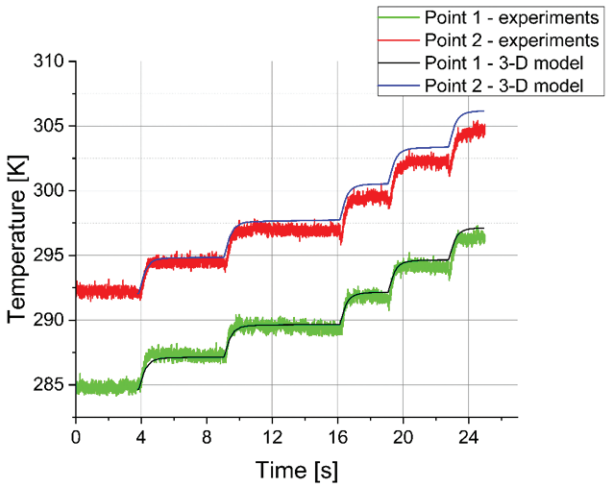

Figure 16. 3-D model simulation temperature, single shot scenario.

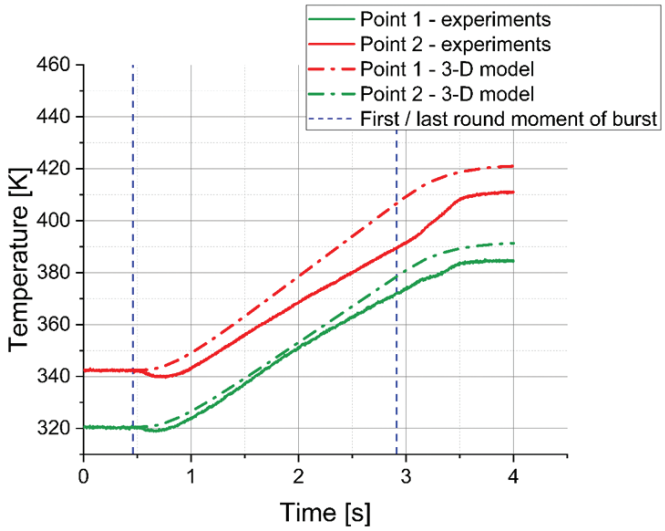

Figure 17. 3-D model simulation temperature, full burst scenario.

3.1.3.2 Full Burst Scenario

The same steps with those described for single shot were executed, but with the next differences

- The initial temperature distribution through the gun barrel, that was about 320 K on Point 1 and 342 K on Point 2;
- The cooling Transient Thermal module after each round was eliminated;
- Therefore, all the 30 rounds full burst simulation was modelled to run in a single execution;
- The 11 Heat flux components were defined introducing the values contained in Table 2 by 30 times in a row;
- In addition to the 30 rounds full burst Transient Thermal module, a new module was linked to it, in order to compute the cooling process of the gun barrel for a period of 1.1 s, as it can be seen from the experimental results.

For the full burst mode and also for the cooling one, the convective heat transfer coefficient was defined in the same way as it is described for those from the case of single shot simulation. The results of the simulation are revealed in Fig. 17, obtained after a convergence time of approximately 280 hrs.

3.2 Discussion

The comparison between experimental results and numerical results is completed with graphical and statistical methods.

The graphics plot the predicted values against the measured values. Delimitation lines are established to group the data points falling within the sectors related to $Y \leq 0.5 \cdot X$, $0.5 \cdot X < Y \leq X$, $X < Y \leq 1.5 \cdot X$, $1.5 \cdot X < Y \leq 2.0 \cdot X$, and $Y > 2.0 \cdot X$.

The statistical terms and the validation criteria used in[14] are applied in this article. For the single shot scenario, in case of the first point, the predicted results for all methods are compared with the experimental results, graphically in Fig. 18 and statistically in Table 4. Approximately 31% and 68% of the data points are in the regions defined by 0.5X < Y <= 1.0X and 1.0X < Y <= 1.5X, respectively, which means that the predicted results are a little bigger than the experimental results. The statistical values indicate a very good correlation with experimental data in case of all modelling and simulation models, with slightly better results for the 3-D model.

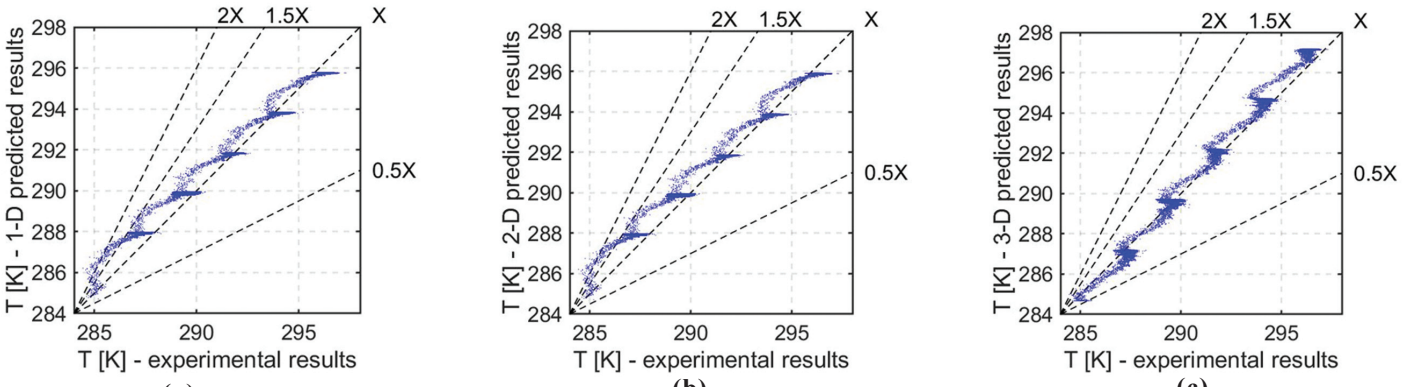

Figure 18. Numerical versus experimental temperature, point 1, single shot scenario: (a) 1-D model; (b) 2-D model; and (c) 3-D model.

Table 4. Statistical data for point 1 temperature, single shot scenario

Coefficient	Experimental results	Numerical results			Relative difference%		
		1-D	2-D	3-D	1-D	2-D	3-D
RMS	290.639	290.880	290.905	290.850	-0.082	-0.091	-0.072
Sk	0.450	0.432	0.448	0.425	4.126	0.555	5.662
Kr	2.098	2.116	2.131	2.088	-0.884	-1.584	0.447
NRMSE	-	0.193 %	0.189 %	0.155 %	-	-	-

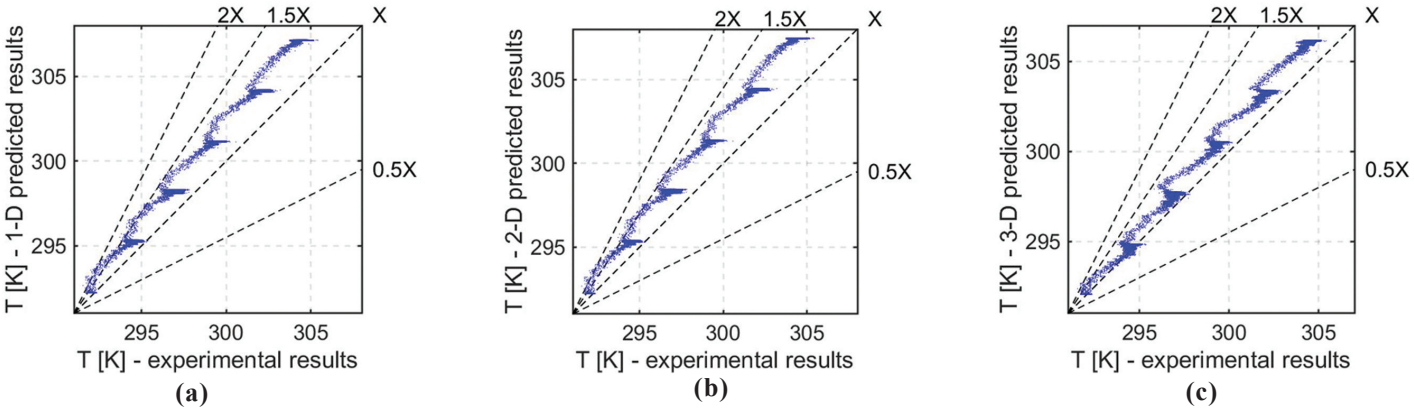

Figure 19. Numerical versus experimental temperature, point 2, single shot scenario (a) 1-D model; (b) 2-D model; (c) 3-D model.

Table 5. Statistical data for point 2 temperature, single shot scenario

Coefficient	Experimental results	Numerical results			Relative difference%		
		1-D	2-D	3-D	1-D	2-D	3-D
RMS	298.158	299.687	299.850	298.985	-0.512	-0.567	-0.277
Sk	0.450	0.449	0.449	0.428	0.09	0.235	4.881
Kr	2.103	2.101	2.101	2.088	0.067	0.081	0.686
NRMSE	-	0.554%	0.613%	0.319 %	-	-	-

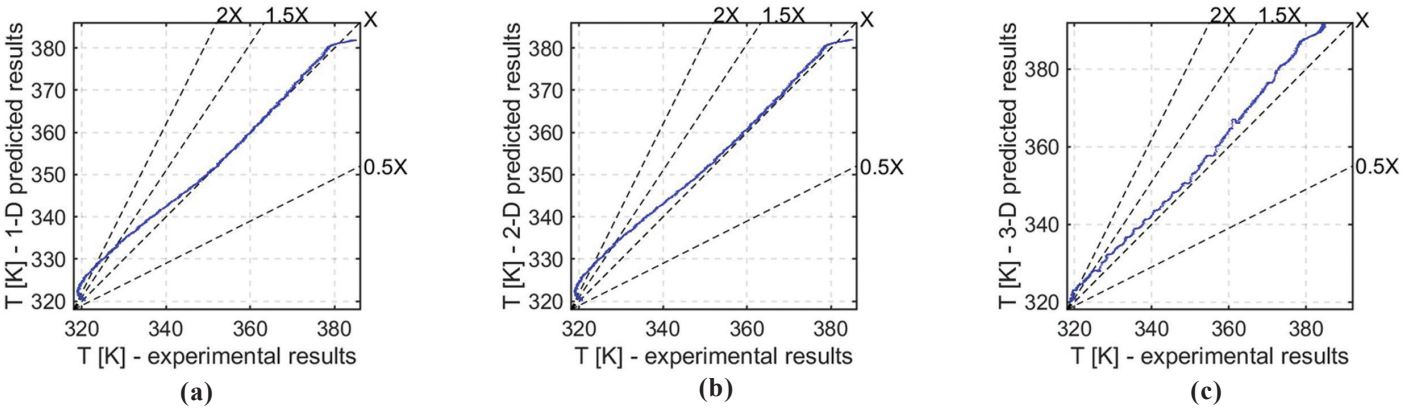

Figure 20. Numerical versus experimental temperature, point 1, full burst scenario: (a) 1-D model; (b) 2-D model; and (c) 3-D model.

For the single shot scenario, in case of the second point, the predicted results for all methods are compared with the experimental results, graphically in Fig. 19 and statistically in Table 5. Most of the data points fall in 1.0X < Y <= 1.5X sector, which means that the predicted results overestimate the measured results. Still, the statistical values indicate a good correlation with experimental data in case of all modelling and simulation models, with slightly better results for 3-D model.

For the full burst scenario, in case of the first point, the predicted results for all methods are compared with the experimental results, graphically in Fig. 20 and statistically in Table 6. The predicted results almost overlap the experimental results, the statistical data confirming the good correlation obtained for this case.

For the full burst scenario, in case of the second point, the predicted results for all methods are compared with the

Table 6. Statistical data for point 1 temperature, full burst scenario

Coefficient	Experimental results	Numerical results			Relative difference%		
		1-D	2-D	3-D	1-D	2-D	3-D
RMS	355.106	356.135	356.527	359.435	-0.289	-0.400	-1.219
Sk	-0.167	-0.175	-0.209	-0.116	-4.757	-24.753	30.551
Kr	1.611	1.628	1.646	1.575	-1.052	-2.158	2.257
NRMSE	-	0.722 %	0.774 %	1.318 %	-	-	-

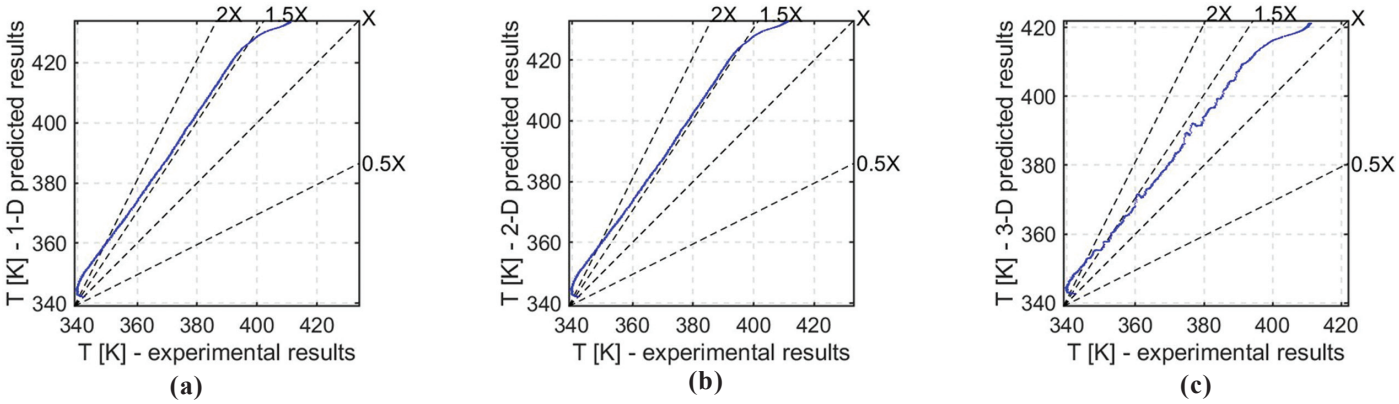

Figure 21. Numerical versus experimental temperature, point 2, full burst scenario (a) 1-D model; (b) 2-D model; (c) 3-D model.

Table 7. Statistical data for point 2 temperature, full burst scenario

Coefficient	Experimental results	Numerical results			Relative difference%		
		1-D	2-D	3-D	1-D	2-D	3-D
RMS	375.065	393.412	392.845	385.607	-4.89	-4.740	-2.810
Sk	0.080	-0.144	-0.140	-0.117	280.349	275.087	246.195
Kr	1.686	1.603	1.602	1.575	4.946	5.009	6.623
NRMSE		5.005 %	4.854 %	2.916	-	-	-

experimental results, graphically in Fig. 21 and statistically in Table 7. Most of the data points are in 1.0X < Y <= 1.5X and 1.5X < Y <= 2.0X sectors, which means that the predicted results overestimate the measured results in a greater extent. Still, the statistical values indicate an acceptable correlation with experimental data, with the exception of *Sk* value, which reflects different asymmetries. One reason for *Sk* relative difference magnitude is the fact that *Point 2* is near the gas ejection port, which is not considered by the thermodynamic interior ballistic model. Another reason for *Sk* extent is due to the cumulative error generated by the small error remarked at the single shot scenario.

4. CONCLUSIONS

In this article, new experimental and computing methods were presented in details in order to determine the external surface temperature of the small arms weapon systems barrel. The experimental tests were conducted on a PA 5.45 mm cal. assault rifle, but can be easily applied to other gun, without any weapon modification, since external sensors were used for measurements. The two infrared thermometers and the shock wave microphone allowed to exactly establish the moment of each shoot. In this way, the surface temperature variation over time is clearly associated with the rate and mode of fire, the advantage of the new procedure over processes mentioned in other articles being obviously. For numerical simulations, the initial conditions were established based on STANREC 4367 thermodynamic interior ballistic model. The heat transfer was solved for one-dimensional and two-dimensional model using the finite difference discretization method, with code written in Matlab software.

The three-dimensional model was resolved by finite element analysis method in Ansys software. Two firing scenarios were analysed, single shot and full burst, with measurements in two different points. The agreement between theoretically and experimentally determined external surface temperatures proved the good applicability of the modelling and simulation methods for computing the heating of the small arms weapon systems barrel under single shot and full burst. The three-dimensional model generated the best results in detriment of computing time. Still, the entire work provides scientific base for the study of new barrel materials, for the small arms weapon systems barrel life prediction, for other non-destructive tests or for determining the cook-off conditions and safety establishing the infantry live-fire training plans. One of the three models presented in this paper can be chosen in accordance with the precision expectation and the available computer resources.

REFERENCES

1. Xu, D.; Luo, Y. & Wenbo, F. The temperature field

pattern of small caliber automatic gun. *In* 4th International Conference on Sensors, Mechatronics and Automation (ICSMA 2016), Advances in Intelligent Systems Research, 2016, **136**, 551-556.
doi: 10.2991/icsma-16.2016.96

2. Ghanem, M.; Abdelsalam, O.; Guirgis, S. & Aboel Khair, M.S. Solution of heat transfer problem for thick walled automatic weapon barrel subjected to continuous firing. *In* Int. J. 17th International Conference on Aerospace Sciences & Aviation Technology, ASAT – 17, 2017.
3. Elbe, R. External barrel temperature of the M16A1 rifle. Technical Report, Small Arms Weapons Systems Directorate, Rock Island Arsenal, Rock Island, Illinois 1975.
4. Bicen, A.R.; Khezzar, L.; Schmidt, M. & Whitelaw, J. H. Heat transfer and velocity characteristics of single- and two-phase flows in a subsonic model gun. Exp. Heat Transfer. J. *Therm. Energy Generation, Transport, Storage, and Conversion.*, 1989, **2**(4), 333-352.
doi: 10.1080/08916158908946372
5. Akçay, M. & Yükselen, M.A. Unsteady thermal studies of gun barrels during the interior ballistic cycle with non-homogenous gun barrel material thermal characteristics. *J. Therm. Sci. Technol*., 2014, 75 – 81.
6. Ghanem, M. & Abdelsalam, O. Transient heat transfer for GPMG's barrel 7.62x51mm. *In* IOP Conf. Series: Materials Science and Engineering 973 012032, May 30-June 3, 2021. doi: 10.1088/1757-899X/973/1/012032
7. Chen, T.C. & Liu, C.C. Inverse estimation of time-varied heat flux and temperature on 2-D gun barrel using input estimation method with finite-element scheme. *Def. Sci. J.,* 2008, **58**(1), 57-76. doi: 10.14429/dsj.58.1623
8. Feng, G.T.; Zhou, K.D.; Zhang, Y.Q.; He, L.; Li, J.S. & Wang, J. The study of gun barrel's two-dimensional nonlinear thermal conduction. *I. J. Thermophys.,* 2019, **40**(4). doi: 10.1007/s10765-019-2502-8
9. Evci1, C.; & Işık, H. Analysis of the effect of propellant temperature on interior ballistics problem. *J. Therm. Eng.*, 2018, **4**(8), 2127-2136.
doi: 10.18186/journal-of-thermal-engineering.433738
10. STANREC 4367: Thermodynamic interior ballistic model with global parameters. NATO Standardization Office, 2016.
11. Akin, J.E. 13 Concepts of thermal analysis. FEA Concepts. SW Simulation Overview, 2009, 190-210.
12. Qian, Q.; Wang, Q. & Wang, C. Influence of meshing on thermal effect simulation of laser irradiation. IOP Publishing, IOP Conference Series: Materials Science and Engineering 2019.
doi: 10.1088/1757-899X/782/3/032063
13. Yuzhao, Y.; Xiaozun, Z.; Cheng, X. & Fan, L. Dynamic stress analysis of anisotropic gun barrel under coupled thermo-mechanical loads via finite element method. *Lat. Am. J. Solids Struct.,* 2020.
doi: 10.1590/1679-78255800
14. Roşca, P.; Mărmureanu, M.; Ţigănescu, V.; Pîrvulescu, C.; Bîndac, I.; & Doru, C. Determination of tyre-ground interaction parameters through image processing in Matlab. *Int. J. Heavy Vehicle Systems.*, 2021, **28**(5).
doi: 10.1504/IJHVS.2021.10037338

ACKNOWLEDGEMENT

This work was supported by a grant of the Ministry of Research, Innovation and Digitization, CNCS/CCCDI – UEFISCDI, project number PN-III-P2-2.1-PED-2019-1981, within PNCDI III.

CONTRIBUTORS

Dr Marius-Ionuţ Mărmureanu obtained his PhD degree in Aerospace Engineering from University Politehnica of Bucharest. He is working at Military Equipment and Technologies Research Agency (METRA), Romania. His research interests include: Ammunitions, exterior ballistics and interior ballistics modeling.
In the current study he performed the 1-D and 2-D heat transfer simulation, the thermodynamic interior ballistic model and drafted the paper.

Dr Petru Roşca obtained PhD degree in Mechanical engineering, from Military Technical Academy, Bucharest, Romania. He is currently working in Military Equipment and Technologies Research Agency (METRA), Romania. His research interests include: Armoured vehicles and armament systems.
In the current study he coordinated the experimental activities and provided guidance on simulation model development and pre-processing of experimental data.

Mr Cristian Predoi obtained his master's degree in System Engineering from University Politehnica of Bucharest. He is currently working in Military Equipment and Technologies Research Agency (METRA), Romania. His research interests include: Weapons and ballistic systems.
In the current study he performed the experimental activities and drafted the paper.

Mr Constantin-Cristinel Puică obtained his master's degree in Genius Engineering Systems from Military Technical Academy, Bucharest, Romania. He is currently working in Military Equipment and Technologies Research Agency (METRA), Romania. His research interests include: Finite Element Analysis.
In the current study he performed the 3-D heat transfer simulation.

Mr Adrian Malciu obtained his master's degree in Special Mechanical Systems Engineering for defense and security from Military Technical Academy, Bucharest, Romania. He is currently working in Military Equipment and Technologies Research Agency (METRA), Romania. His research interests include: Ballistic protection and finite element analysis.
In the current study he performed the 3-D heat transfer simulation and drafted the paper.

Mr Gabriel-Flavius Noja obtained his B.E. in Ammunition, Rockets, Explosives and Propellants from Military Technical Academy, Bucharest, Romania. He is currently working in Military Equipment and Technologies Research Agency (METRA), Romania. His research interests include: Interior ballistics modeling.
In the current study he performed the 1-D and 2-D heat transfer simulation and drafted the paper.